JOURNAL OF MATERIALS SCIENCE **38** (2003) 2011 – 2018

Titanium oxy-nitride films deposited on stainless steel by an ion beam assisted deposition technique

K. YOKOTA, K. NAKAMURA, T. KASUYA, S. TAMURA, T. SUGIMOTO, K. AKAMATSU, K. NAKAO
High Technology Research Center and Faculty of Engineering, Kansai University Suita, Osaka 564-8680, Japan
E-mail: kyokota@ipcku.kansai-u.ac.jp

Surfaces of stainless steel SUS304 were coated with titanium oxy-nitride (TiON) films at temperatures of 400– 770°C using an ion-beam assisted deposition technique constructed from an electron beam evaporator for Ti evaporation and a microwave ion source for ionizing nitrogen gas. The N ions were accelerated at energies of 0.5–2.0 keV. Most of the deposited TiON films consisted of (60–80)% TiN and (40–20)% TiO_2, and the fraction of TiO_2 increased with increasing substrate temperature. Hardness of the TiNO films varied in the range from 160 GPa to 260 GPa with increasing substrate temperature. The titanium oxy-nitride film could be deposited on stainless steel without a significant deterioration surface layer at 600°C. However, when TiNO films were deposited at temperatures higher than 700°C, the thickness of the TiNO films were significantly thinner and a thick layer containing nitride such as Cr_2N, CrFe, Fe_2N and Fe_4N was formed in a near surface region of stainless steel because more nitrogen diffused into stainless steel.

1. Introduction

Stainless steel is an important material because of high corrosion resistance. However, its hardness is not sufficient for covering wide application. This disadvantage can be improved by coating the surface of stainless steel with hard thin films such as titanium nitride (TiN). Titanium nitride belongs to the family of refractory transition metal nitrides and is an important material in advanced metallization area for ultralarge scale integrated circuits [1, 2] and in surface protective coating engineering for steels [3, 4].

Physical vapor deposition (PVD) technique is used to coat the surface of stainless steel with hard films such as TiN at low temperatures. Coating at low temperatures is required to avoid a phase transformations of stainless steel during hard film coating. On the other hand, the hardness of TiN films increases with increasing substrate temperature [5]. To ensure a fully dense and well-adhered hard coating at low temperatures, hard coating processes involve ion assisted deposition, such as low-voltage electron beam evaporation [6], triode high-voltage electron beam evaporation [7], and magnetron sputtering [8], etc. Ionized elements can energetically migrate on the film surface to promptly find favorable sites although the ion-bombardment introduces more damages into the films [9]. The damages serve to improve hardness of the films [10]. However, plenty of oxygen even in a deposition chamber with a low background vacuum such as $\sim 10^{-5}$ Pa could be present. Titanium atoms reacted readily with oxygen remaining in the chamber because the Gibbs's free energy for TiO_2 is smaller than that for TiN [11] and as a result titanium oxide is contained in deposited TiN films. The hardness of TiN_xO_y films was not so high as that of TiN films [12].

In this paper, we searched substrate temperature and nitrogen ion-beam energy suitable for coating the surface of stainless steel with very hard thin TiNO films without significant deterioration of stainless steel using an ion-beam assisted deposition technique.

2. Experimental details

Ion beam assisted deposition (IBAD) used for this experiment was constructed basically from an electron beam evaporator for Ti evaporation and a microwave ion source for N ionization as shown in Fig. 1. Ionized N particles were extracted from the microwave ion source at energies of 4–6 keV, and decelerated by an electrode located in front of the extraction electrode. The nitrogen ion-beam energy is the difference in applied voltage between the deceleration electrode and the extraction electrode. The beam intensity was held constant to 0.1 mA/cm^2 by voltages applied to the deceleration electrode and the extraction electrode. A substrate holder was continuously rotated to coat uniformly the surfaces of stainless steel with a hard film. The background pressure was about 4×10^{-5} Pa. The surfaces of

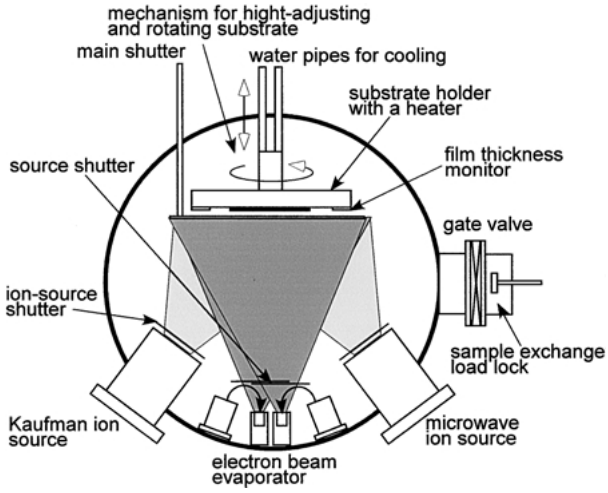

Figure 1 Schematic of the ion beam assisted deposition (IBAD) apparatus used in this experiment.

stainless steel were coated with TiNO films in vacuum of $\sim 10^{-2}$ Pa at substrate temperatures of 400–770°C for 60 min. Nitrogen gas of 25 sccm was fed into the microwave ion source. Fine lapped austenite stainless steel SUS304 was successively rinsed in alcohol, acetone, and solvent naphtha, and was charged into the apparatus immediately after rinsing with deionized water. Table I is a list of the samples prepared with various N ion-beam energies and various substrate temperatures.

The prepared samples were examined using X-ray diffraction (XRD) with the Cu K_α radiation in Seeman-Bohlin geometry at an incident angle of 7°. The diffraction angle was measured with an accuracy of 1/64 deg. The XRD peaks were assigned to crystal lattice planes by referring the powder diffraction file [13]. The chemical bonding state of each element was analyzed by an X-ray photoelectron spectroscopy (XPS) technique using a monochromatic Mg K_α (1353.6 eV) radiation source. Argon ion-beam sputtering was used for investigating the chemical bonds in the greater region of the films. The XPS signals were measured with an energy resolution of about 1 eV. Then, the samples were analyzed with Rutherford backscattering spectrometry (RBS) that He ions with energy of 2.0 MeV are used as a probe beam. The detection angle was adjusted to 165° and the angle of incidence was adjusted to 60° for analyzing a depth resolution operation of about 10 nm. The spectra were simulated using the computer code RUMP [14]. The thickness of the deposited films was measured using a laser probe roughness tester with a depth resolution of 0.02 μm. The surface morphology of the prepared samples was studied using an atomic force microscope (AFM). Hardness tests were performed in the range from 1 gf to 150 gf at a rate of 0.2–2.4 gf/s using a dynamic ultra microhardness tester (Shimazu DUH-W201). For each samples, more than 10 hardness measurements were made to assure sufficient confidence in resulting data.

TABLE I A list of samples

	N^+ ion energy (keV)			
Substrate temperature (°C)	0.5	1.0	1.5	2.0
400	1	2	3	4
500	5	6	7	8
600	9	10	11	12
700	13	14	15	16
770	17	18	19	20

3. Measurement of hardness of thin films on substrates

Now, an indenter is advancing into a sample with a testing load as shown in the insert in Fig. 2. The sample consists of a material with a hardness of H_s and a thin film with a hardness of H_f and with a thickness of δ. The indenter breaks the thin film, is subsequently advancing with increasing the testing load, and stopped at a depth of $d (D = d + \delta)$ in the substrate when the testing load reached the setting value of W_m. At that time, the hardness tester exhibited a hardness of H_m. Here, the thickness δ of the thin film is enough thin as compared with the depth d of the indenter advanced into the substrate. Hardness H is defined as W/S, where W is the test load weight and S is the contact area between the indenter and the sample. After the indenter broke the thin film, the indenter is subsequently advancing into the substrate with resistance due to abrasive wear for the thin film and deformation of the thin film. We assume that the thin film keeps elasticity during the hardness measurement. The testing load is divided to the thin film and the substrate, respectively, as follows: $W_m = H_m S_m = kH_f S_f + H_s S_s$, where k is a constant relating to abrasive wear resistance and deformation of the thin film, and the suffixes, f and s, show the thin film and the substrate, respectively. Hardness is linearly proportional to abrasive wear resistance with a constant of 1.3α as a relative value to TiC [15], where α is a constant. The area of the thin film contacting with the indenter after broken can be approximated as an equation of $S_f/S_m = \{\gamma(d+\delta)^2 - \gamma d^2\}/S_m \fallingdotseq 2\gamma d\delta/\gamma d^2 = 2\delta/d \fallingdotseq 2\delta/D$ since $S_m \fallingdotseq S_s$. Here, γ is a constant determined with the shape of the indenter. Thus, we can approximate as $H_m S_m \fallingdotseq H_f S_f - H_s S_m$. Hardness can be represented as an equation of $(H_m - H_s) \fallingdotseq (2k\delta H_f)$

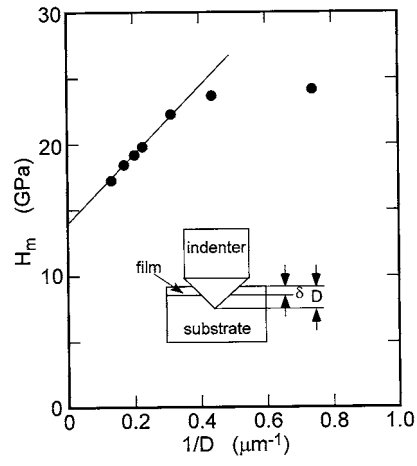

Figure 2 A relationship between H_m and $1/D$ measured under various testing load for the No. 6 sample. The insert is a model for calculation of hardness for a thin film deposited on a substrate.

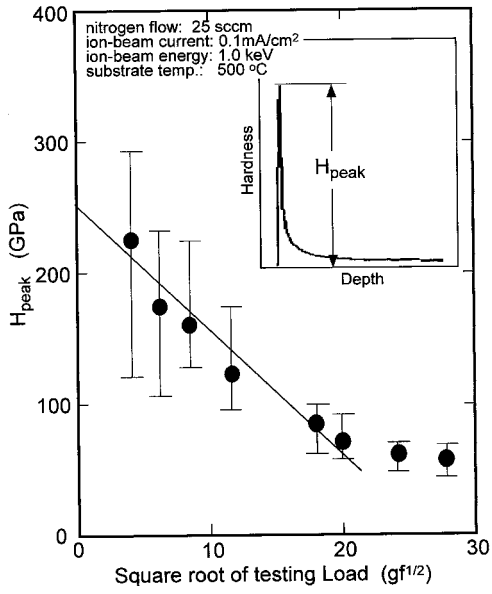

Figure 3 A relationship between hardness H_{peak} and the square root of setting-testing load for the No. 6 sample.

$(1/D)$ as a function of the depth. Thus, the hardness of the thin film can be obtained from the slope $(2k\delta H_f)$ of the $(H_m - H_s)$ vs. $1/D$ straight line.

The indenter was advanced into the samples with a rate of 0.1–2.4 gf/s, increasing with an increase in the setting-testing load. The hardness vs. depth curves is measured with the approximately same duration for any testing load. The indenter passes through the TiNO film and advances into the substrate. The value of H_{peak}, as shown in the insert in Fig. 3, reflects a value near the hardness of the TiNO film at the very beginning of the measurement. However, the hardness tester shows a value of H_{peak} smaller than the hardness of the TiNO film with an increase in the testing load because of a finite response of the hardness tester and an increase in the advanced speed of the indenter. The advancing rate of the indenter into the material becomes fast with an increase in the testing load. When hardness H for a material is measured with various testing loads W, the depth D is proportional to the square root of the testing load since $H = W/S$ and $S = \gamma D^2$. Thus, the advancing rate of the indenter into the material is proportional to the square root of the testing load, and the value of H_{peak} is inversely proportional to the square root of the setting-testing load. Fig. 3 shows values of H_{peak} as a function of the square root of the setting-testing load. The measured values varied widely with decreasing the setting-testing load since the surfaces of the deposited TiNO films were in an irregular rough state. The values of H_{peak} were inversely proportional to the square root of the setting-testing load, and becomes close to a small hardness corresponding to that of the substrate, with larger setting-testing load. The hardness of the deposited TiNO film can be obtained by extrapolating to the longitudinal axis (H_{peak} axis). On comparison of the hardness ($H_f = 250$ GPa) extrapolated to the zero testing load and the hardness ($k\ H_f = 13$ GPa μm/$\delta(\mu$m$) = 43.3$ GPa (as $\delta = 0.3\ \mu$m)) obtained from the slope of the $(H_m - H_s)$ vs. $1/D$ straight line as shown in Fig. 2, the value of k can be calculated as about 0.17. For many samples, the k values were around 0.17, varying from 0.15 to 0.18. This value of k was used through this experiment.

4. Experimental results and discussion

4.1. Crystallographic structures

Fig. 4 shows X-ray diffraction patterns as a function of N ion-beam energy and substrate temperature for representative samples. Two large XRD peaks from the (111) and (200) planes of stainless steel and three small XRD peaks from the (111), (200), and (220) planes of TiN were observed for all of samples. The samples prepared at 770°C had more small peaks in addition to diffraction peaks from TiN and stainless steel. The small X-ray diffraction peaks are assigned to hydrogen carbon nitride (HCN) such as $C_7H_6N_4$ and $C_2H_5N_5$, CrFe, and metal carbide $M_{23}C_6$. Rivlin [16] found that the hydrogen carbon nitrides are produced in a near surface region of stainless steel when stainless steel was treated in nitrogen atmosphere at high temperatures.

The deposited TiN films are polycrystals oriented to ⟨111⟩, ⟨200⟩, and ⟨220⟩ directions. The intensities of the XRD peaks became larger with increasing substrate temperature. The deposited TiNO films had approximately the same intensity ratio of $I(220)/I(111)$ of 0.8 although the ratios of $I(200)/I(111)$ varied in the range from 0.7 at 400°C to 2.1 at 770°C, increasing with increasing substrate temperature. However, the TiNO film deposited at 600°C only had a large $I(200)/I(111)$ of 3.1. We had no reasons for the large ratio for the TiNO film deposited at 600°C. Furthermore, on the No. 12 sample that was prepared with the N ion-beam energy of 2 keV, the XRD peaks from the (200) plane were very small and were disappearing in a shoulder of the large XRD peak from the (111) plane of SUS 304 with

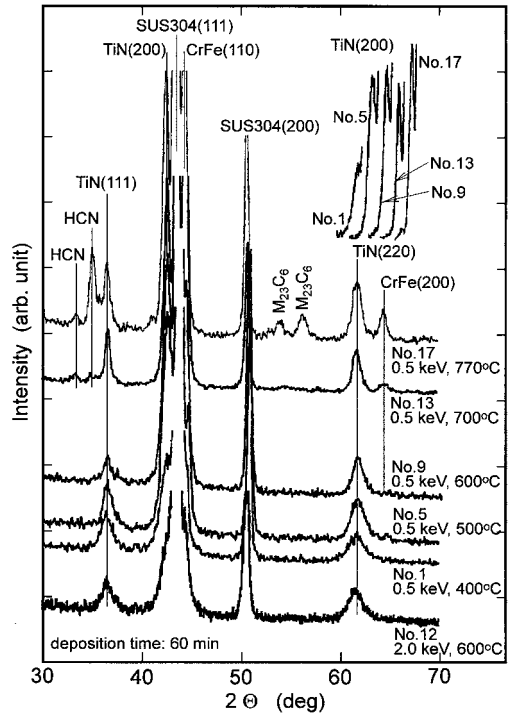

Figure 4 X-ray diffraction patterns as a function of N ion-beam energy and substrate temperature for representative samples.

increasing substrate temperature. Polycrystalline TiN in the JCPDS card [13] has the preferentially oriented (200) plane and the ratio of $I(200)/I(111)$ was 1.4. However, Ando *et al.* [17] showed that TiN films deposited on (100) Si substrates using an ionized vapor deposition technique at energies of 100–1000 eV were preferentially oriented to the ⟨200⟩ direction with increasing ion energy. It is known that TiN preferentially oriented to the ⟨111⟩ direction grew in equilibrium conditions with low strain energy [18] and TiN orientated to the ⟨100⟩ direction grew in nonequilibrium conditions with high surface energy [19]. Pelleg *et al.* [20] showed that TiN films were preferentially oriented in the order following ⟨200⟩, ⟨220⟩, and ⟨111⟩ directions with increasing film thickness because stress in films is released with increasing film thickness. The ion-beam energy dependence of the preferential orientation in this experiment differed from other experiment results. This fact was resulted from the difference in deposition temperature: the TiN films in the above references have been deposited on substrates at substrate temperatures lower than 300°C while the substrate temperatures in this experiment were higher than 400°C. Thus, it seems that stress induced into TiNO films by irradiation of energetic N ion particles was released because of high substrate temperatures.

Fig. 5 shows lattice plane spacing of the deposited TiNO films as a function of N ion-beam energy and substrate temperature. The (200) lattice plane spacing depended scarcely on N ion-beam energy and substrate temperatures in a range of temperatures lower than 600°C although that of TiNO films deposited at 700 and 770°C became slightly small. The (220) lattice plane spacing depended scarcely on N ion-beam energy and substrate temperature. However, the deposited TiNO films were preferentially oriented to the (111) lattice plane, strongly depending on substrate temperature. The TiNO films deposited at 400°C consisted of unit cells expanded to the ⟨111⟩ direction by about 1%, as compared with the (111) lattice plane spacing (0.24492 nm) in the JCPDS card [13]. The (111) lattice plane spacing became smaller with increasing substrate temperature although it was scarcely dependent on N ion-beam energy. Ion-beam assisted deposition technique leaves significantly stress in the deposited films [9, 10]. Many of TiN films already reported [17–20] have preferentially oriented to the (200) lattice plane because of larger remaining stress since they were deposited onto substrates at temperatures lower than 300°C. However, in this experiment, substrate temperatures were higher than 400°C, and the deposited TiNO films were not preferentially oriented to the (200) lattice plane. These film depositions were performed with N ions with the almost same energy. To release affects of ion bombardment on the film surface, the deposited films had either the preferential oriented lattice plane or the larger (111) lattice plane spacing substrate. The remaining stress in the deposited films finds to be released with increasing substrate temperatures since the (111) lattice plane spacing come close up 0.24492 nm in the JCPDS card [13] with increasing substrate temperature.

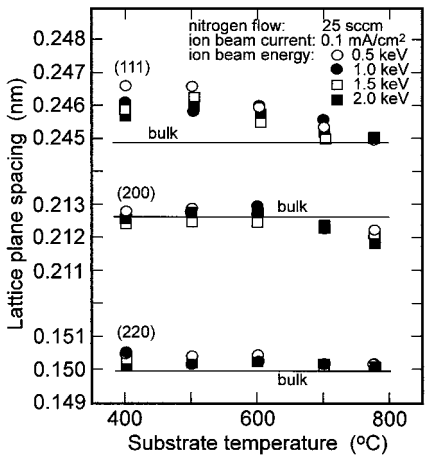

Figure 5 Lattice spacing of deposited cubic TiN containing in the deposited films as a function of N ion-beam energy and substrate temperature.

4.2. Compositional and chemical structures

Fig. 6 shows the X-ray photoemission spectra measured on the surfaces prepared by removing the thickness of about 50 nm from the surface of the No.9 and No.14 samples that TiN films were deposited at 600 and 700°C, respectively. The Ti $2p_{3/2}$ and Ti $2p_{1/2}$ peaks, the N $1s_{1/2}$ XPS peak, and the O $1s_{1/2}$ XPS peak were not observed at binding energies of 455 and 461 eV, 399 eV, and 532 eV, respectively, for isolated elements [21]. The Ti $2p_{3/2}$ peak and Ti $2p_{1/2}$ peak for the No.9 and No.14 samples were measured at binding energies of 456 and 462 eV as corresponding to those in TiN, respectively, the N $1s_{1/2}$ peak was measured at a binding energy of 396.8 eV as corresponding to that in TiN, and the O $1s_{1/2}$ peak was measured at a binding energy of 531.2 eV as corresponding to that in TiO_2 [22, 23]. The line shapes of the N $1s_{1/2}$ and the O $1s_{1/2}$ XPS signals can be reproduced with one Gaussian component. However, the line shapes of the Ti $2p_{3/2}$ and the Ti $2p_{1/2}$ XPS signals could not be reproduced with two

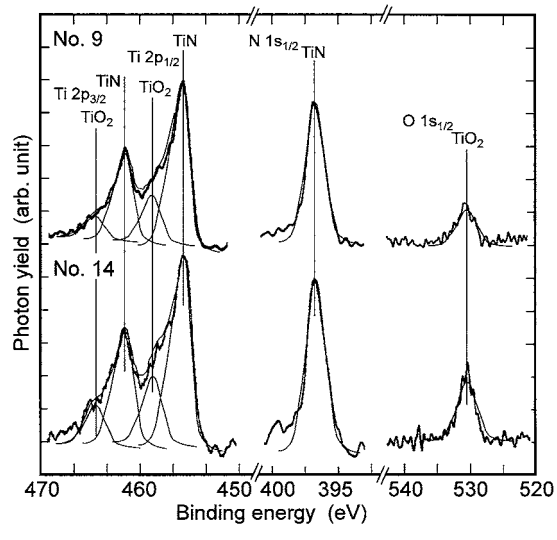

Figure 6 X-ray photoemission spectra measured on the surfaces prepared by removing the thickness of about 50 nm from the surface of the No. 9 and No. 14 samples. The fine solid lines show Gaussian components used to reproduce the measured XPS line.

Gaussian components as corresponding to the two signals. To reproduce entirely the measured line shapes of the Ti XPS signals, two Gaussian components with the centroid energies at 459 eV for the Ti $2p_{1/2}$ XPS signal and at 464.9 eV for the Ti $2p_{3/2}$ XPS signal were required to use together with the Ti $2p_{1/2}$ and Ti $2p_{3/2}$ XPS signals corresponding to TiN. The 459 eV Ti $2p_{1/2}$ and the 464.9 eV Ti $2p_{3/2}$ XPS signals show that TiO_2 contains in the TiN films [22, 23]. The TiO_2 component in the TiN films is a result that Ti atoms reacted readily with oxygen remaining in the chamber because the Gibbs's free energy for TiO_2 is smaller than that for TiN [11]. Thus, we refer the deposited films to as TiNO. Titanium oxy-nitride films deposited by a hollow cathode reactive DC sputtering system had relatively larger XRD peaks at twice diffraction angles of 41.9° and 43.1° in addition to 42.59° corresponding to the diffraction peak from the (200) plane of TiN and XRD peaks at twice diffraction angles of 61.2° and 62.4° in addition to 61.8° corresponding to the diffraction peak from the (220) plane of TiN [12]. The TINO films deposited in this experiment had no additional XRD peaks as described above. It seems that titanium-oxide in this experiment is not crystallized and precipitates in the vicinity of grain-boundaries of TiN.

Fig. 7 shows the backscattered He^+ ion spectra and the compositional structures of representative three samples prepared at substrate temperatures of 600°C, 700°C, and 770°C, respectively. The compositional structures were determined by considering the above XPS measurement results showing the presence of TiO_2 in the deposited films since the sensitivity of RBS for light elements such as N and O atoms in silicon is very

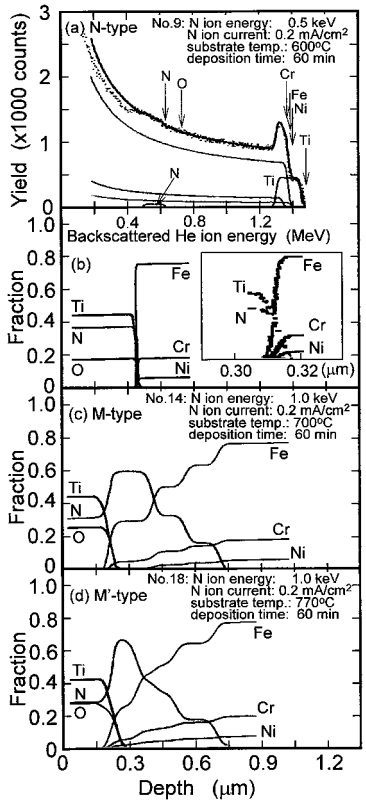

Figure 7 Measured backscattered He^+ ion spectra and the compositional structures of representative samples.

low. The compositional structures for the samples prepared at 600°C, 700°C, and 770°C referred to as N-type, M-type and M′-type, respectively. The compositional structures of samples were strongly dependent on substrate temperature although they were scarcely dependent on N ion-beam energy. These compositional structures for the prepared samples were also confirmed by the XPS measurement. Here, we did not show the XPS results.

For the N-type samples, it finds that the surface of stainless steel was covered with a TiNO film consisting of about 80% TiN and about 20% TiO_2 without a significantly modified surface of stainless steel. The M-type samples had TiNO films consisting of about 70% TiN and about 30% TiO_2 accompanying a significantly modified surface of stainless steel. Nitrogen diffused into a near surface region of stainless steel, and three characteristic terraces in the constituent profile were formed in the region. The diffusion coefficient of N atoms was 6.5×10^{-11} (cm^2/s) in stainless steel at 400°C [24]. For the No. 14 sample, the diffusion length $2(Dt)^{1/2}$ of N atoms in the stainless steel was only 0.6 μm smaller than 10 μm at 400°C for 60 min. The retardation of the N atom diffusion in stainless steel is because of the nitridization of stainless steel. Compounds such as Cr_2N, Fe_2N, Fe_4N, and Ni_3N are estimated as nitrides of constituent atoms in stainless steel from the Gibbs's free energy [11]. The M′-type samples had TiNO film consisting of about 67% of TiN and about 33% of TiO_2. The chrematistic composition steps between the TiNO film and the substrate became unclear compared with the M-type sample because the compounds such as $M_{23}C_6$ and CrFe, as shown in Fig. 4, were formed in the same region and nitride such as Cr_2N, Fe_2N, Fe_4N, and Ni_3N was decomposed at a temperature of 770°C.

4.3. Thickness of TiNO films

Fig. 8 shows the thickness of TiNO films deposited for 60 min as a function of N ion-beam energy and substrate temperature. The thickness of TiNO films decreased with increasing N ion-beam energy although it became significantly thinner at a temperature between 600 and 700°C. At temperatures above 700°C, TiNO films became thinner because nitrogen diffuses significantly into stainless steel as shown in Fig. 7, and a layer consisting of nitride such Cr_2N, Fe_2N, Fe_4N, and Ni_3N was formed in a near surface region of stainless steel at the high temperatures. The thickness of the deposited TiNO films decreased as the thickness of the modified surface layer of stainless steel, obtained from Fig. 7, increased. The relationship was shown in the insert in Fig. 8. The thickness of deposited films became thinner with increasing ion-beam energy at a rate of 0.18 nm/eV for the TiNO film deposited at temperatures lower than 600°C, 0.05 nm/eV for that at 700°C, and 0.02 nm/eV for that at 770°C: the films were sputtered with the rates during deposition. We considered for the ion-beam energy dependence of the sputtered rate as a follows. The maximum energy loss for the incident N ion-beams is in a head-on collision with atoms with the same mass:

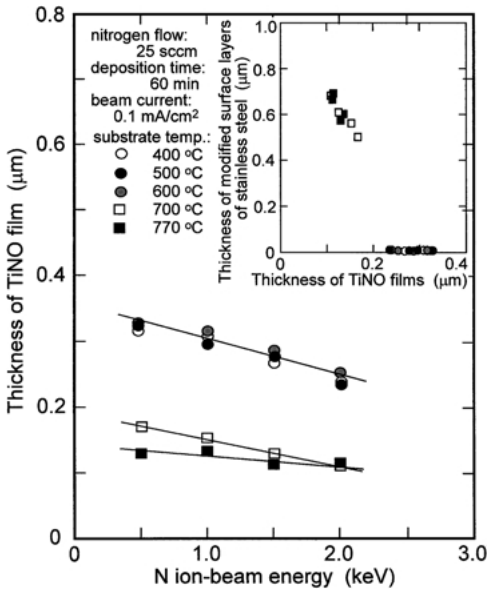

Figure 8 The thickness of TiNO films as a function of N ion-beam energy and substrate temperature. The insert shows a relationship between the thickness of deposited TiNO films and the thickness of a N atom-diffused region (a near surface region in stainless steel).

the N ion-beams are easy to sputter the TiNO films with a large fraction of TiN. The fraction of TiO_2 in the deposited TiNO films increased with increasing substrate temperature as shown in Fig. 7.

4.4. Hardness of TiNO films and stainless steel

Fig. 9 shows the hardness H_f for the deposited films, calculated from the slopes of the straight lines on the relationship between H_m and $1/D$, as a function of substrate temperature and nitrogen ion-beam energy. The hardness for deposited TiNO films was strongly dependent on N ion-bean energy rather than substrate temperature in the range from 160 to 260 GPa. The hardness for the TiNO films increased with increasing N ion-beam energy, and decreased after reached maximum at 1 keV regardless of substrate temperature. The deposited TiNO films had hardness compared with that

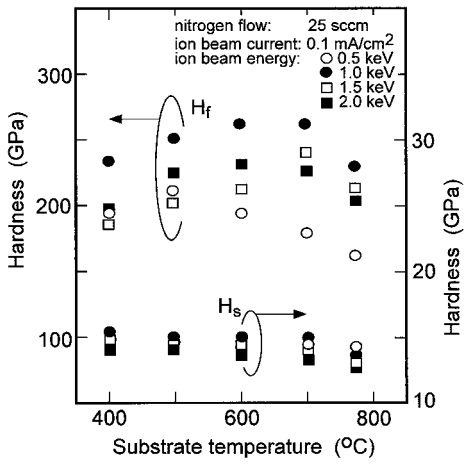

Figure 9 Hardness for TiNO films and substrates (stainless steel) as a function of substrate temperature and nitrogen ion-beam energy.

for TiN films prepared using technique assisted by energetic ion-beams [19]. However, the hardness of the deposited TiNO films was about two times larger than about 170 GPa for bulk TiN [26] and about two hundred times larger than those of the TiN_xO_y films deposited by a hollow cathode reactive DC sputtering system [12]. The large hardness of the deposited TiNO films in this experiment may be because the additional XRD peaks hinting the presence of TiN_xO_y crystals as described above [12] were not observed on the deposited TiNO films. The deposited TiNO films had approximately the same intensity ratio of $I(220)/I(111)$ of 0.8 while the ratios of $I(200)/I(111)$ increased from 0.7 at 400°C to 2.1 at 770°C with an increase in substrate temperature. The TiNO film deposited with 1 keV at 600°C had hardness of about 1.1 times larger than 235 GPa for that deposited at 400°C. The hardness of the deposited TiNO films increased with an increase in N ion-beam energy and decreased after reached a maximum at 1 keV while the ratios of $I(200)/I(111)$ decreased significantly with an increase in N ion-beam energy. Our experiment results did not follow to the

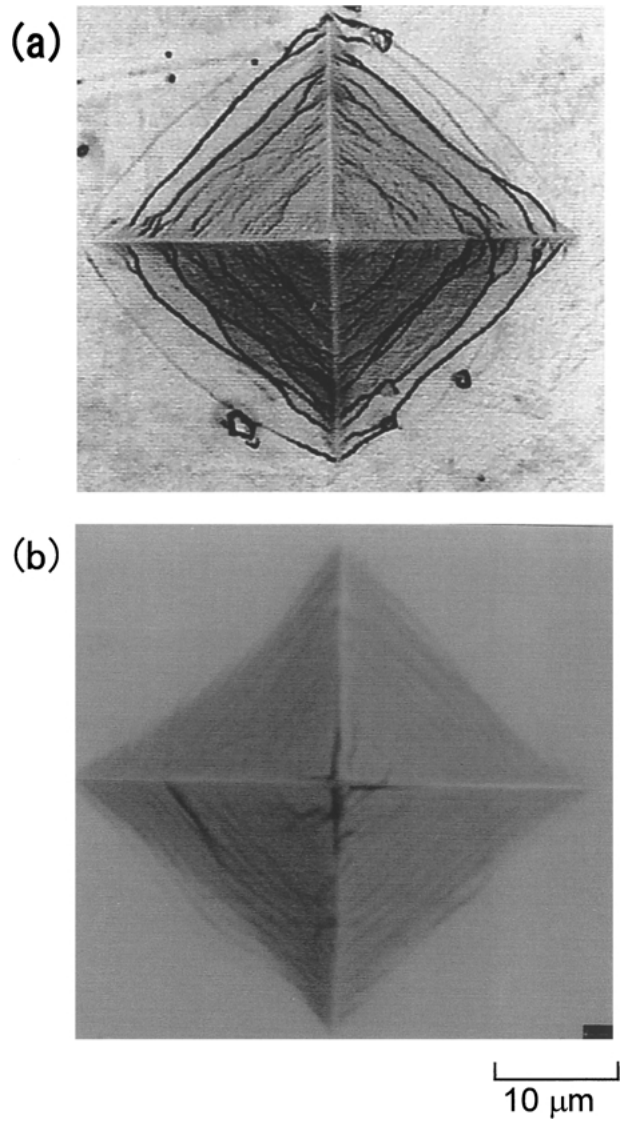

Figure 10 Indenter abrasions after the hardness test for 1 μm thickness TiN films deposited on stainless steel using a conventional CVD technique and the IBAD technique, respectively.

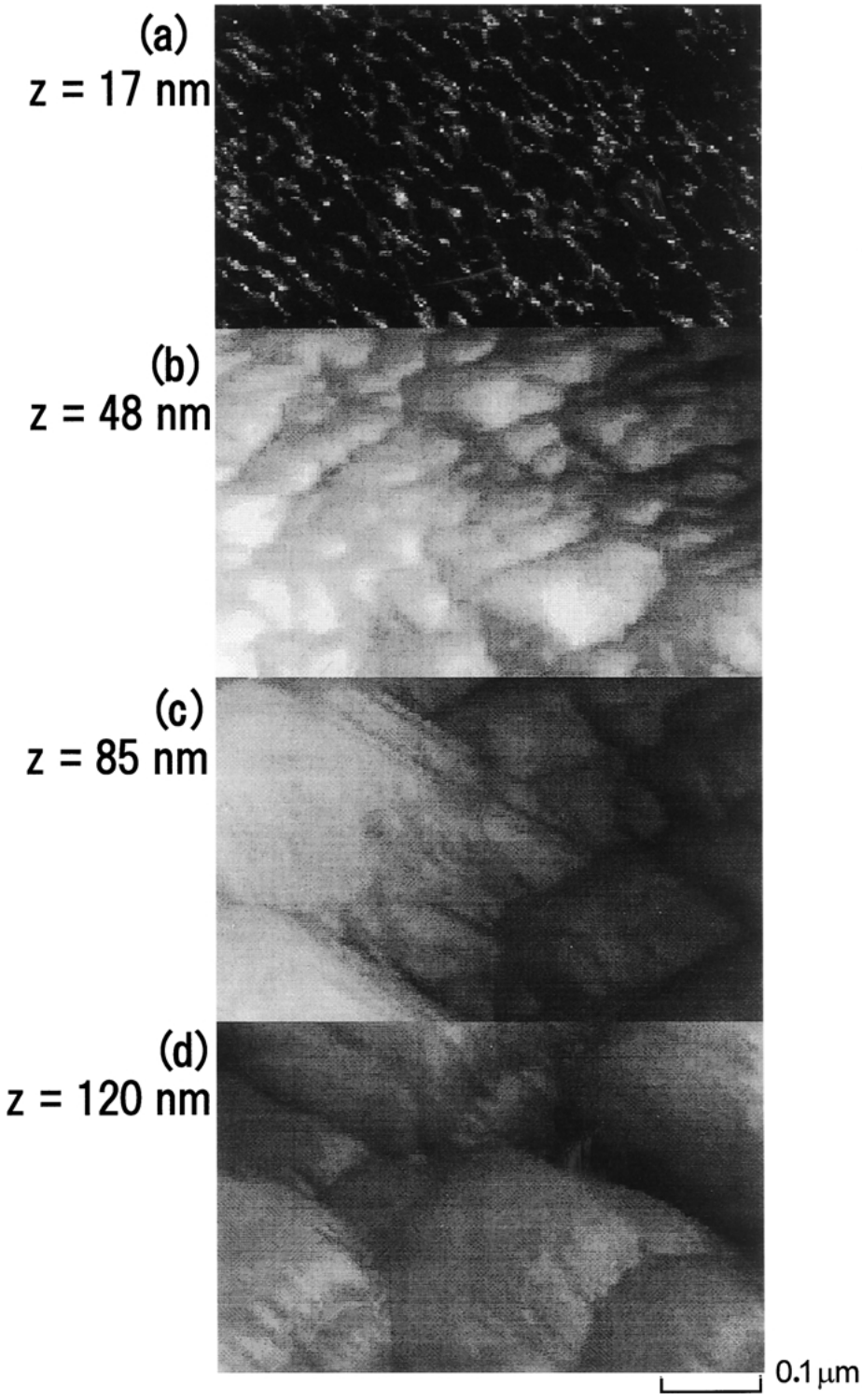

Figure 11 The AFM photography on the surfaces of TiNO films deposited on stainless steel as a function of substrate temperature and N ion-beam energy: (a) No.10 sample, (b) No.14 sample, (c) No. 15 sample, and (d) No. 16 sample. The value of z shows maximum roughness for the sample surfaces.

relationship between hardness and preferential orientation as already known. However, on film deposition with N ion-beam energies lower than 0.5 keV, the deposited TiNO films have large stress accompanying to orientate to the ⟨200⟩ and ⟨220⟩ directions [10]. The surfaces of the TiNO films were sputtered by bombardment of energetic N ions while deposition, and the thickness of the sputtered TiNO film increased with increasing the N ion-beam energy. Furthermore, the intensities of X-rays diffracted from the TiNO films became significantly smaller with increasing N ion-beam energy as shown in Fig. 4: more radiation damages were left in the TiNO films under higher N ion-beam energy deposition. The amount of the radiation damages increase with increasing the N ion-beam energy although some radiation damages are annealed out for the film deposition at high substrate temperatures: this suggests a suitable amount of damages to improve hardness of the films [10]. In this experiment, a TiNO film with a suitable amount of damages was deposited with the N ion-beam energy of 1 keV.

Substrates used for low temperature TiNO film deposition had approximately the same hardness as stainless steel [25]. However, the hardness decreased slightly with increasing N ion-beam energy and with increasing substrate temperature since more nitride with a small hardness such as Fe_2N [26] was formed a near surface region of stainless steel. Fig. 10 shows indenter abrasions observed using an atomic force microscope after the hardness measurement for 1 μm thickness TiN films deposited on stainless steel at 400°C using a conventional chemical vapor deposition (CVD) technique and the IBAD technique, respectively. The IBAD TiNO film was deposited with the N ion-beam energy of 0.5 keV. The CVD film surface had many clear cracks while the IBAD TiNO film had scarcely cracks.

4.5. Surface morphology

Fig. 11 shows AFM photography for the TiNO films deposited on stainless steel as a function of substrate temperature and N ion-beam energy. The surfaces of TiNO films deposited at substrate temperatures below 600°C were rugged as shown in Fig. 12a, and their surface morphologies did not vary with N ion-beam energy. Although the surfaces were rugged, the maximum roughness z was only 17 nm. When substrate temperature increased from 600°C to 700°C, the surfaces of the deposited TiNO films were gradually waved compared with that of the low temperature TiNO film as shown in Fig. 12b–d. The waves in the TiNO films became larger with increasing N ion-beam energy, and the surface roughness also increased. The roughness reached 120 nm for the sample deposited at 700°C and at 2 keV. The significant change in the TiNO film surface morphology was well corresponding to the production of carbide such as $M_{23}C_6$ and CrFe and nitride such as Cr_2N, CrFe, Fe_2N and Fe_4N in the near surface region of the stainless steel. The samples prepared at 770°C had approximately the same AFM photography as those prepared at 700°C. The surface roughness of TiNO films in this experiment was far larger than the surface roughness of 2.5 nm on the TiN_xO_y films deposited by a hollow cathode reactive DC sputtering [12].

5. Conclusion

Titanium nitride was deposited on stainless steel using the IBAD technique. The thickness of the deposited films decreased with increasing substrate temperature and decreased with increasing N ion-beam energy because the surfaces of the deposited films were sputtered by collision of energetic N ions. The deposited titanium nitride films consisted of TiN and TiO_2, and the fraction of TiO_2 in the films increased with increasing substrate temperature. The formation of TiO_2 is because Ti atoms reacted with oxygen remaining in the chamber. Carbide such as $M_{23}C_6$ and CrFe and nitride such as Cr_2N, CrFe, Fe_2N and Fe_4N were formed in a near surface region of the stainless steel while deposition at temperatures higher than 700°C. The formation of the nitride was because nitrogen diffused into stainless steel and carbide was due to an intrinsic change of stainless steel self. The deposition rates of the TiNO films were small at substrate temperatures higher than 700°C because of the diffusion of nitrogen into stainless steel. Hardness for the deposited TiNO films increased with increasing substrate temperature, and decreased after reached the maximum hardness of 260 GPa for the TiNO film deposited at 600°C. The hardness of the TiNO films deposited at high substrate temperatures became smaller because the fraction of TiO_2 in the TiNO films increased. A TiNO film with large hardness can be deposited with the N ion-beam energy of 1 keV as a result of radiation damages introduced by bombardment of N ion-beams and of recovery of the radiation damages during the film deposition.

This research was supported in part by the research support organization of Institution of Industrial Technology of Kansai University.

References

1. N. KUMAR, K. POURREZAEI, B. LEE and E. C. DOUGLAS, *Thin Solid Films* **164** (1988) 417.
2. H. JOSWIG, A. KOHLHASE and P. HUCHER, *ibid* **175** (1989) 17.
3. J. P. BUCHER, K. P. ACKERMANN and F. W. BUSCHOR, *ibid.* **122** (1984) 63.
4. J. S. CHO, S. W. NAM and P. HUCHER, *J. Mater. Sci.* **17** (1982) 2495.
5. M. KOMIYA, ION NITRIDING and ION CARBORIZING (eds.) "Materials Science Society of Japan, Surface Treatment in Materials" (Shokabo, Tokyo, 1966) p. 131.
6. E. MOLL and H. DAXINGER, US Patent no. 4,197,175 (April 8, 1980).
7. A. MATTHEWS and D. G. TEER, *Thin Solid Films* **80** (1981) 41.
8. W. D. MUNZ, *Surf. Coat. Technol.* **48** (1991) 81.
9. A. MATTHEWS, K. FANCEY, A. S. JAMES and A. LEYLAAND, *ibid* **61** (1993) 121.
10. J. PELLEG, L. Z. ZEVIN and S. LUNGO, *Thin Solid Films* **197** (1991) 11.
11. O. KUBASCHEWSKI and C. B. ALCOCK, "Metallurgical Thermochemistry" (Pergamon, Oxford, 1979) Tables.
12. M. H. KAZEMEINI, A. A. BEREZIN and N. FUKAHARA, *Thin Solid Films* **372** (2000) 70.
13. Joint Committee for Powder Diffraction Standards, Powder Diffraction File (International Center for Diffraction Data, Park Lane).
14. L. R. DOOLITTLE, *Nucl. Instrum. Methods Phys. Res.* **B9** (1985) 344.
15. M. H. KHRUSHCHEF and M. A. BABICHEV, *Friction and Wear of Machine* **9** (1987) 22.
16. V. G. RIVLIN and G. V. RAYNOR, *Int. Met. Rev.* **25** (1987) 21.
17. Y. ANDO, K. OGATA, H. YAMAKI and S. SAKAI, *Nucl. Instr. and Meth.* **B39** (1989) 158.
18. S. VEPREK, *Thin Solid Films* **130** (1985) 135.
19. J. E. SUNDGREN, *ibid* **128** (1985) 21.
20. J. PELLEG, L. Z. ZEVIN and S. LUNGO, *ibid.* **197** (1991) 117.
21. A. D. BAKER and D. BETTERIDGE, "Photoelectron Spectroscopy" (Pergamon, New York, 1972) Appendix 2.
22. W. Y. YANG, H. IWAKURA, H. YAGI, T. KURODA and S. NAKAMURA, *Jpn. J. Appl. Phys.* **23** (1984) 1560.
23. "Simadzu Data Handbook" (Simadzu, Kyouto, 1980) Table 1.
24. N. YASUMARU, *J. Japan Inst. Metals* **61** (1997) 424.
25. D. R. LIDE, "Handbook of Chemistry and Physics," 80th ed. (CRC, Boca Raton, 1999) 12.
26. Japan Institute of Metals, Data Book for Metals (Maruzen, Toukyo, 1987) p. 128.

Received 7 March 2002
and accepted 21 January 2003